ORIGINAL RESEARCH

Size Matters: Ryanodine Receptor Cluster Size Affects Arrhythmogenic Sarcoplasmic Reticulum Calcium Release

Samuel Galice, PhD;* Yuanfang Xie, PhD;* Yi Yang, PhD;* Daisuke Sato, PhD;† Donald M. Bers, PhD†

Background—Ryanodine receptors (RyR) mediate sarcoplasmic reticulum calcium (Ca^{2+}) release and influence myocyte Ca^{2+} homeostasis and arrhythmias. In cardiac myocytes, RyRs are found in clusters of various sizes and shapes, and RyR cluster size may critically influence normal and arrhythmogenic Ca^{2+} spark and wave formation. However, the actual RyR cluster sizes at specific Ca^{2+} spark sites have never been measured in the physiological setting.

Methods and Results—Here we measured RyR cluster size and Ca^{2+} sparks simultaneously to assess how RyR cluster size influences Ca^{2+} sparks and sarcoplasmic reticulum Ca^{2+} leak. For small RyR cluster sizes (<50), Ca^{2+} spark frequency is very low but then increases dramatically at larger cluster sizes. In contrast, Ca^{2+} spark amplitude is nearly maximal even at relatively small RyR cluster size (≈10) and changes little at larger cluster size. These properties agreed with computational simulations of RyR gating within clusters.

Conclusions—Our study explains how this combination of properties may limit arrhythmogenic Ca^{2+} sparks and wave propagation (at many junctions) while preserving the efficacy and spatial synchronization of Ca^{2+}-induced Ca^{2+}-release during normal excitation-contraction coupling. However, variations in RyR cluster size among individual junctions and RyR sensitivity could exacerbate heterogeneity of local sarcoplasmic reticulum Ca^{2+} release and arrhythmogenesis under pathological conditions. **(*J Am Heart Assoc*. 2018;7:e008724. DOI: 10.1161/JAHA.118.008724.)**

Key Words: calcium regulation • calcium signaling • calcium sparks • ryanodine receptor

Ryanodine receptors (RyRs) mediate calcium (Ca^{2+}) release from the sarcoplasmic reticulum, an essential process in the activation of striated muscle contraction. RyR sensitivity to cytosolic Ca^{2+} ($[Ca^{2+}]_i$) is increased in genetic diseases (catecholaminergic polymorphic ventricular tachycardia), on increased SR Ca^{2+} content, during heart failure, and on certain posttranslational modifications (eg, phosphorylation or oxidation), all of which promote diastolic SR Ca^{2+} leak and triggered arrhythmias.[1] In cardiac myocytes, RyRs form clusters in which some RyRs are tightly packed in checkerboard arrays (corner to corner) with others clustered in a less organized manner within junctional clefts between the SR and sarcolemma.[2-6] These junctional clefts are cylinders 100 to 200 nm in diameter along transverse tubules and surface sarcolemma, with a depth comparable to the height of the RyR protruding from the SR (≈13 nm). The typical junction (of ≈20 000 in a single myocyte) contains 50 to 250 RyRs, mostly along the transverse tubules,[4] and these may correspond to local superclusters.[5] Individual RyR cluster size can vary over a continuous distribution (from <10 up to 250 RyRs), but some smaller clusters are quite close to others (eg, at the same junction) and, because of their proximity (within 100 nm), may function as a single junctional cluster. This proximity explains how a small local Ca^{2+} influx can activate multiple RyRs via Ca^{2+}-induced Ca^{2+}-release (CICR) during the normal action potential–induced Ca^{2+} transient and also during diastolic Ca^{2+} sparks.[7-11] Ca^{2+} sparks are stochastic local CICR events that are typically restricted spatially to 1 cluster/junction without propagation to nearest-neighbor junctions spaced 1.8 to 1.9 μm longitudinally or 0.4 to 0.8 μm transversely.[8-12] This spacing has an important impact on the ability of release at 1 cluster to activate neighboring junctions by CICR to initiate propagating arrhythmogenic Ca^{2+} waves.

Some RyR clusters exhibit Ca^{2+} sparks more frequently than others and could be considered "eager" sites.[11] Such eagerness can be influenced by spatially heterogeneous

From the Department of Pharmacology, University of California, Davis, CA.

Accompanying Figures S1 through S7 are available at http://jaha.ahajournals.org/content/7/13/e008724/DC1/embed/inline-supplementary-material-1.pdf

*Dr Galice, Dr Xie, and Dr Yang contributed equally to this work.

†Dr Sato and Dr Bers are co-senior authors.

Correspondence to: Donald M. Bers, PhD, Department of Pharmacology, University of California, Davis, Genome Building Rm 3513, Davis, CA 95616-8636. E-mail: dmbers@ucdavis.edu

Received February 15, 2018; accepted May 16, 2018.

Clinical Perspective

What Is New?

- Spontaneous Ca^{2+} release from sarcoplasmic reticulum ryanodine receptors (RyR) can induce triggered arrhythmias (eg, via delayed afterdepolarizations).
- The number of RyRs at a given sarcoplasmic reticulum–plasma membrane junction varies widely and may influence the probability of initiating Ca^{2+} spark events.
- We have developed a new method to simultaneously measure both fundamental Ca^{2+} spark properties and the number of RyR molecules at that same site in adult myocytes.
- Both direct measurements and computational modeling demonstrate how Ca^{2+} spark probability at a single site depends steeply on the number of local RyRs, whereas the amount of Ca^{2+} released is surprisingly independent of RyR number.

What Are the Clinical Implications?

- In a healthy heart, this combination of junctional release site properties can limit arrhythmogenic Ca^{2+} wave propagation while preserving spatially uniform synchronous Ca^{2+} release during the normal heartbeat.
- However, in pathological states (eg, heart failure), enhanced spatial variations in RyR cluster size and sensitivity may perturb this balance and exacerbate arrhythmogenesis.

posttranslational modifications (eg, RyR phosphorylation or oxidation[13]), but relatively rapid Ca^{2+} diffusion inside the SR network makes it less likely that heterogeneity would exist for local intra-SR $[Ca^{2+}]$ ($[Ca^{2+}]_{SR}$),[14,15] which, like local cleft $[Ca^{2+}]_i$, is a major regulator of RyR gating.[16] Moreover, the relationships between Ca^{2+} sparks and $[Ca^{2+}]_{SR}$ depletion events at a given site are often self-similar but vary widely among sites.[17] This suggested a structural rather than a simple stochastic basis for differences in local Ca^{2+} spark properties among release sites. Because the probability that a single RyR opening can trigger a full-blown Ca^{2+} spark via CICR depends on recruitment of multiple near neighbors at a given junction,[18] the number of RyRs at a single junction might have an implicit effect on the eagerness of a given junction to produce Ca^{2+} sparks or to promote arrhythmogenic Ca^{2+} waves.

Here we test the hypothesis that RyR cluster size influences Ca^{2+} spark frequency using both direct experimental measurements of RyR cluster size and Ca^{2+} sparks as well as computational simulations. We used our well-characterized experimental system, which allows simultaneous confocal visualization in live myocytes of Ca^{2+} sparks and the number of local RyRs.[9] In this method we fluorescently label virtually all RyR monomers with FKBP12.6 that is covalently tagged with a small red fluorescent probe (F-FKBP) in the same cell where Ca^{2+} sparks are measured. We have previously quantified that F-FKBP binds to RyR in situ with high affinity (K_d<1 nmol/L) and ≈1:1 binding stoichiometry per RyR monomer, with only a slight influence on Ca^{2+} spark properties.[9] Thus, we can measure the relative number of RyRs at each site where Ca^{2+} sparks occur. To test our quantitative understanding of this relationship, we also use our detailed mathematical model of stochastic RyR opening at individual junctions that has allowed us to characterize the local CICR synergy involved in Ca^{2+} spark genesis.[18]

Materials and Methods

The data, analytic methods, and study materials will be made available to other researchers for purposes of reproducing the results or replicating the procedure.

The data that support the findings of this study are available from the corresponding author on reasonable request.

Myocyte Preparation

Adult Sprague-Dawley rats were euthanized, and their ventricular cardiac myocytes were isolated using previously described methods.[9] Briefly, anesthesia (isoflurane, 5%) and heart excision were followed by 5 minutes of perfusion (37°C) with minimal essential medium (MEM, GIBCO Life Technologies) gassed with 95% O_2/5% CO_2 before collagenase B (0.5 mg/mL, Boehringer Mannheim, Mannheim, Germany) and protease (0.02 mg/mL, Sigma, St. Louis, MO) were added to dissociate myocytes. Isolated myocytes were incubated (37°C) in the same MEM solution, washed, and held at 100 μmol/L Ca^{2+} until use. The care of the animals and procedures were approved by the University of California, Davis Animal Research Committee in accordance with the NIH Guide for the Care and Use of Laboratory Animals. After saponin-induced permeabilization (50 μg/mL for 3 minutes) myocytes were then perfused for 10 minutes with internal solution containing 50 nmol/L free $[Ca^{2+}]$.[19] Experiments were performed at room temperature (25°C).

Fluorescent Labeling of Single-Cysteine Mutant of FKBP12.6

A single-cysteine mutant of the human small immunophillin FK-506–binding FKBP12.6 isoform (T14C-FKBP12.6) was labeled by the thiol-specific maleimide derivative of Alexa Fluor® 568 (Invitrogen, Carlsbad, CA), as previously described.[20] This F-FKBP binds to and regulates RyRs in SR vesicles and permeabilized myocytes such as wild-type FKBP12.6.[9]

Confocal Microscopy

Experiments were performed on a high-speed, 2-dimensional (2D) microscope (Zeiss, Oberkochen, Germany, LSM 5 Live) equipped with a C-Apochromat 63×/1.2 numerical aperture objective (Zeiss). The 2D frame mode with 512×512-pixel resolution was used. Due to trade-offs of spatial versus temporal resolution, we used the same zoom factor for simultaneous Ca^{2+} spark and initial F-FKBP recordings.[9] Afterward, we increased zoom factor and measured Z-stack image of F-FKBP fluorescence to refine analysis of RyR density and distribution. We used information from lower-zoom F-FKBP images to refine alignment of higher-zoom-factor Z-stack images. This improved the precision of RyR imaging at Ca^{2+} spark sites.

Measurements of F-FKBP Fluorescence

Z-line–bound F-FKBP in Z-stack images was recorded after incubation of the permeabilized cardiac myocytes in 100 nmol/L T14C-FKBP12.6 that had been labeled with red fluorescent Alexa 568 (see extended methods in Guo et al[21]). At this [F-FKBP], RyR monomers should be 99.3% saturated with F-FKBP. For each cell, 2 zoom factors were applied. The first zoom factor was set to 0.8, which produced an x-y pixel size of 0.26×0.26 μm. A second zoom factor (2.0) provided an x-y pixel size of 0.10×0.10 μm. Measurements were taken from 40 optical slices (of 0.64 μm) on average. F-FKBP was excited with a DPSS (Santa Clara, CA) 532-nm laser with emission measured after a 600-nm long-pass filter.

Measurements of Ca^{2+} Sparks

Ca^{2+} sparks time series were measured using Fluo-4 (25 μmol/L) in 2D imaging. The intracellular solutions contained (in mmol/L): EGTA 0.5, HEPES 10, K-aspartate 120, free $MgCl_2$ 1, ATP 5, reduced glutathione 10, phosphocreatine di-Tris 10, creatine phosphokinase 5 U/mL, dextran (Mr 40 000) 4%, at pH 7.2 with total [Ca^{2+}] required to obtain the desired 50 nmol/L free [Ca^{2+}] (using MaxChelator). These conditions were chosen to allow Ca^{2+} sparks but to prevent Ca^{2+} waves because the presence of Ca^{2+} waves complicates Ca^{2+} spark quantification (eg, waves can suppress subsequent Ca sparks for some time). We selected cells from which background fluorescence was relatively constant and in which spontaneous global Ca^{2+} waves were absent. Fluo-4 was excited with a Sapphire 488-100 laser, and emitted fluorescence was detected with a 530±15 nm filter. The zoom factor was set to 0.8, producing an x-y pixel size of 0.26×0.26 μm. The scan speed was set at 12.5 ms/frame, and 600 frames were recorded on average at the single selected cell middle z-plane.

Automated Ca^{2+} Spark Detection and Localization

For Ca^{2+} spark analysis, we developed an algorithm that is quite similar to 2 prior 2D Ca^{2+} spark analysis methods.[22,23] Our approach is based on local detection of Ca^{2+} sparks by applying a threshold to the region of the image occupied by the cell. Briefly, we first filtered the 2D frame time series using inverse Fast Fourier Transform with high-frequency removal to eliminate horizontal stripes and pseudoperiodic patterns, which favored better Ca^{2+} spark detection. For each 2D frame time series, a binary mask of the cell was created to match only Ca^{2+} sparks within the cytosol (excluding nucleus and perinuclear regions). Then, all scan images were normalized using a time-dependent basal fluorescence to correct for slow temporal drifts in signal. A 2D Gaussian filter was then applied to enhance image structures at different scales. Ca^{2+} sparks were detected from the normalized images by using a custom segmentation method based on a threshold-dependent rule using 1 SD from the quiescent masked region of the cell. Then, further detection criteria such as spark mass (mean intensity) and peak amplitude evolution were automatically adapted to experimental parameters. Finally, all detected sparks were visually validated to limit obvious false positives. Very-small-amplitude SR Ca^{2+} release events or single RyR openings surely occur (as a non-spark-mediated Ca^{2+} leak),[16,18] but are missed events here. We employed an ellipsis fit to estimate the morphology of Ca^{2+} sparks at their peak intensity: location, peak amplitude, major and minor axes. Then, the distance from the Ca^{2+} spark peak at its highest-intensity locus to the nearest RyR cluster center was measured.

Image Processing

Image analysis used ImageJ[24] plugins and custom Python (http://www.python.org/) scripts combined with SciPy (http://www.scipy.org/) and NumPy (http://www.numpy.org/) modules. We used the Richardson-Lucy deconvolution algorithm to improve the quality of F-FKBP Z-stack images. This algorithm is available as an ImageJ plugin in (DeconvolutionLab[25]) and can be used effectively when the point-spread function (blurring operator) is known. We used another ImageJ plugin, PSF Generator,[26] to create a synthetic point-spread function based on our optical system characteristics as input parameters and used the generated point-spread function to sharpen image restoration.

RyR Cluster Size Measurement

For each detected RyR cluster, the size was estimated based on the mean F-FKBP fluorescence intensity within a disk diameter of 0.5 μm and from previously obtained

characteristics of distributions of RyRs per cluster. Cluster estimates deduced from our confocal images suggest that the mean size is ≈84 RyR channels (see Results).

Statistical Analysis

The data presented in this article were obtained from 5 different rats, with the number of animals (N) and cells (n) indicated as appropriate in the figure legends. Data were fit either to linear regression or nonlinear regression analysis (eg, Gaussian or Lorentzian for histograms) as indicated in text and figures. Analyses were performed using GraphPad Prism 5 software (La Jolla, CA).

Mathematical Model Overview

Computer simulations were carried using a detailed ventricular cell model with spatial Ca^{2+} dynamics, as previously implemented by our group.[18] In this model each RyR is formulated in a 4-state Markovian model and regulated simultaneously by $[Ca^{2+}]$ in both the dyadic cleft ($[Ca^{2+}]_{cleft}$) and SR luminal ($[Ca^{2+}]_{SR}$). Instead of the fixed number of the RyR cluster size in the original model, we investigated the effect of RyR cluster size ranging from 1 to 250, as indicated by experimental data.[27] Increases of $[Ca^{2+}]_i$ of 200 nmol/L ($\Delta[Ca^{2+}]$, versus baseline) were used for Ca^{2+} spark detection threshold.

Results

Experimental Measurements of RyR Cluster Size

In individual ventricular myocytes we first measured Ca^{2+} sparks in a time series of 2D scans in 1 central x-y plane in the *Z*-axis, and then RyR cluster size in a Z-stack series of x-y plane scans at different depths (Figure S1). Raw F-FKBP images were first deconvolved using information from the Z-stack of x-y images (as in Figure S2). Figure 1A shows the RyR distribution in an example myocyte x-y plane at which Ca^{2+} sparks were also measured. Yellow spots indicate local F-FKBP maxima. A higher magnification (Figure 1Aa) shows the anticipated transverse striated pattern. This also allowed the identification of putative junctional RyR clusters, differentiated graphically by different colors (Figure 1B). The distribution of the distance between 2 nearest local peaks (Figure 1C) in the longitudinal direction is Gaussian-like with an ≈1.65 μm mean value and narrow full width at half-maximum (green). These data are consistent with expectations for sarcomeric spacing, and the majority of RyRs are located along transverse tubules. In the transverse direction (Figure 1C, red), the mean value is 0.76 μm but with a much broader full width at half-maximum distribution. These distances match expectations based on prior work. On the myocyte periphery, RyR clusters were intercalated between transverse tubules, but that was not apparent for the cell interior (Figure S3A through S3C). We found that the distance between adjacent RyR clusters on the surface had a mean value of ≈0.5 μm, which is smaller than that within the myocyte interior. We also found a helicoid arrangement of RyR-localized z-lines (Figure S3D through S3G), as previously described.[28]

Confocal resolution used here cannot directly resolve individual RyRs within a junctional cluster as is possible with superresolution or electron microscopy.[2-6] However, the relative F-FKBP fluorescence intensity ($\Delta F/F_0$) within 250 nm around the local cluster peak intensity (Figure 1D) provides a direct quantitative readout that is proportional to the number of RyRs within that local cluster (or supercluster; Figure 1E). This F-FKBP fluorescence intensity is linear with [F-FKBP] and has been used to titrate the overall RyR concentration in cardiac myocytes, for comparison to ^{3}H-ryanodine binding data.[9,29]

We used 2 methods to calibrate F-FKBP fluorescence in terms of numbers of RyR (Figure 1E; Figure S4B). First we assume that our mean cluster $\Delta F/F_0$ of 1.39 (Figure 1D) corresponds to the average (or most frequent) RyR cluster size estimated from several prior studies that range mostly between 50 and 150 RyR/cluster, which in some high-resolution cases were clusters of clusters or superclusters.[2-6,27] The mean $\Delta F/F_0$ of 1.39 is indicated by a vertical broken line in Figure 1E. Second, we took a more integrative approach based on the average number of RyR per 1 μm^3 of cytosol from ^{3}H-ryanodine binding maximum (B_{max}) in isolated rat ventricular myocytes (833 fmol/mg myocyte protein).[9] Multiplying this B_{max} by 168 mg myocyte protein/mL cytosol[30] provides an average RyR concentration (84.2/μm^3 cytosol) and the solid line in Figure 1E with slope of 60.6 RyR per $\Delta F/F_0$ unit. This falls well within the range of microscopic estimates (shown by dashed lines for mean values of 50 or 150 RyR/cluster). The inferred number of RyR tetramers per cluster is shown in red on Figure 1D and is used below to convert $\Delta F/F_0$ data to the number of RyRs at individual clusters where Ca^{2+} sparks occur.

Figure 2A shows that the physical size of RyR clusters is also distributed around a mean of 0.0455 μm^2 (equivalent of a circle of 120 nm radius). Not surprisingly, the number of RyRs/cluster correlates with the physical cluster size (Figure 2B), although there is significant variation, which may reflect differences in relative RyR packing.[2,3,5] The clusters were typically asymmetric with the major axis roughly 50% longer than the minor axis (Figure 2C), and the major axis tended to be more transverse in orientation (Figure 2D; Figure S5).

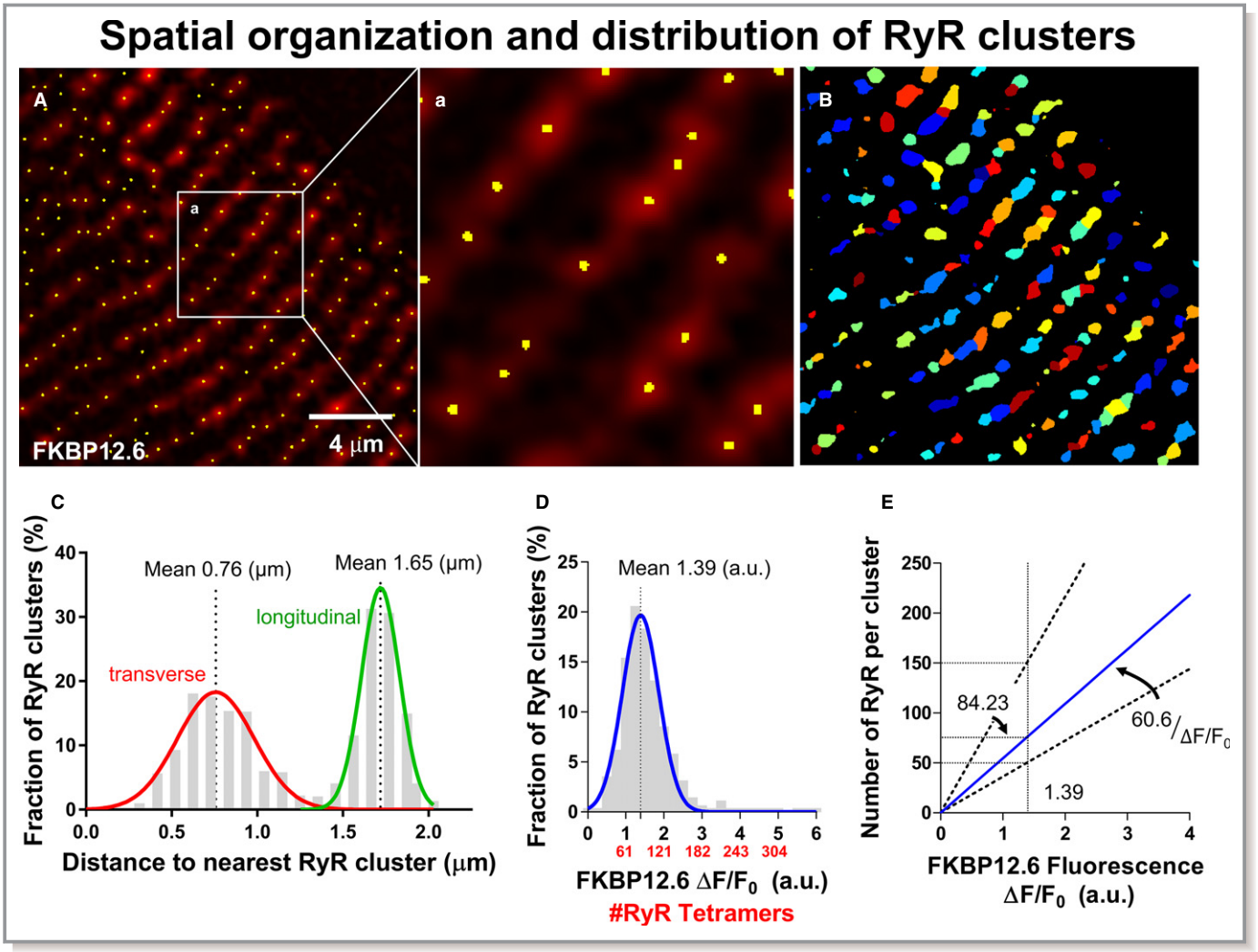

Figure 1. Spatial organization and distribution of ryanodine receptor (RyR) clusters in permeabilized rat ventricular cardiac myocytes. A, Representative confocal F-FKBP12.6 fluorescence image of a rat cardiac myocyte with a 2.0 zoom factor producing an x-y pixel of 0.10×0.10 μm. Each yellow dot represents the local maximum of F-FKBP12.6 fluorescence. Panel a is enlarged part of (A) (white box). B, Labeling of RyR clusters based on a threshold of 90th percentile of the intensity distribution after baseline correction. Different colors were randomly used so that individual clusters could be visibly distinguished. C, Fraction of RyR clusters as a function of the nearest RyR cluster in the transverse direction (red line) and longitudinal direction (green line, Gaussian fits) for the same cell shown in A. D, Fraction of RyR clusters as a function of average F-FKBP12.6 relative fluorescence $\Delta F/F_0$ per cluster (n=10 cells, N=2 rats). Red labels are after translation of $\Delta F/F_0$ to estimated number of RyRs from E. E, Estimation of RyRs per cluster as a function of F-FKBP12.6 relative fluorescence $\Delta F/F_0$. The curve is based on the fact that the mean number of RyRs per cluster (≈84 RyRs) should correspond to the mean of the cluster size from D (1.39 arbitrary unit (a.u.)), with a slope (60.6 RyR/[$\Delta F/F_0$ unit]; see text), allowing the amount of fluorescence in a single cluster to be converted to an estimate of the number of RyR tetramers in that cluster.

Ca^{2+} Spark Detection at Measured RyR Cluster Sites

We developed a new algorithm to automatically detect and analyze Ca^{2+} sparks in 2D time-series images obtained from quiescent cardiac myocytes (Figure 3A shows 1 frame). Small time-dependent changes in local fluorescence occur during recording, and patterns of background fluorescence can limit Ca^{2+} sparks detection in threshold-dependent methods. We minimized these changes by using time-average local cell fluorescence for each pixel, which enhanced Ca^{2+} spark peak detection reliability (Figure 3B). Each raw fluorescence frame is enhanced by subtracting a baseline image lacking Ca^{2+} sparks. Subtraction of the normalized image and the local drift correction removed large variations in background fluorescence for the 5 sparks identified in Figure 3B. We also found that Ca^{2+} sparks are relatively spatially symmetric, as previously reported,[22] but did exhibit some eccentricity (Figure 3C through 3E) comparable to that seen for the RyR cluster shape. It makes sense that the shape of the RyR cluster could influence the shape of the Ca^{2+} spark at that site, although radial diffusion of Ca^{2+} would also be expected to dissipate that shape

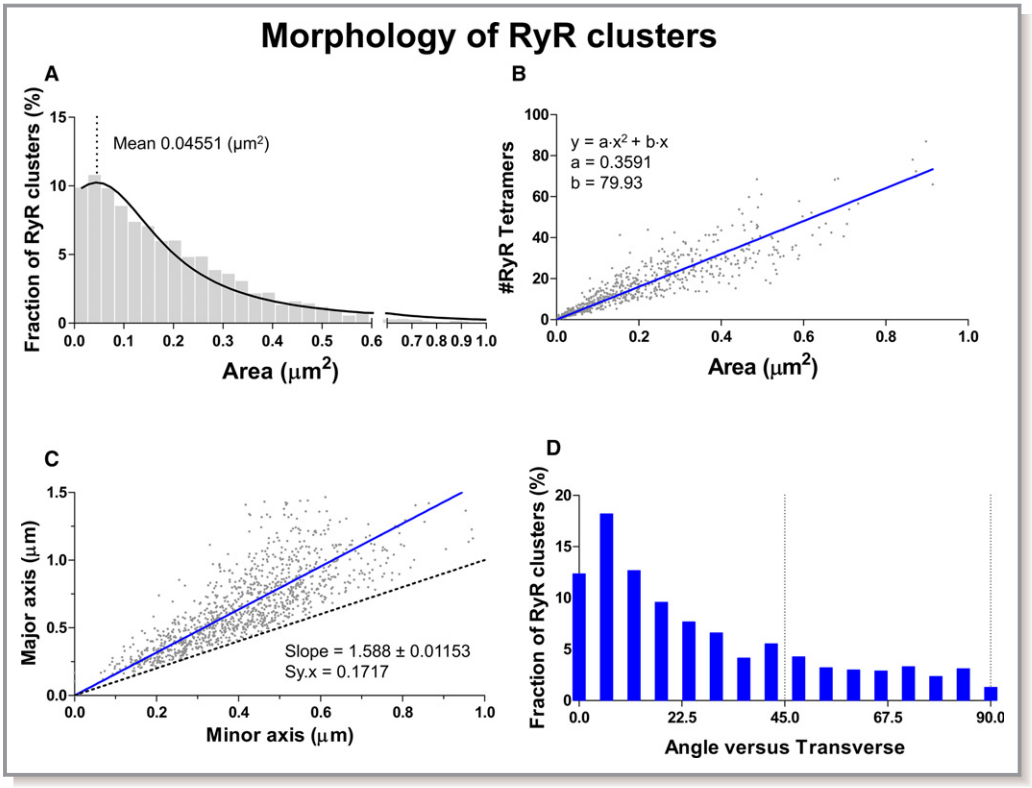

Figure 2. RyR cluster size and shape. A, Histogram of RyR cluster area for images like that in Figure 1B (n=4 cells, N=1 rat, Lorentzian fit). B, Plot of number of RyR tetramers vs physical area for each cluster (n=4 cells, N=1 rat, Quadratic polynomial fit). C, Major vs minor axis for each junctional cluster, with average ratio implied by regression line cluster (n=4 cells, N=1 rat, linear regression). D, The longer (major axis) was more often oriented along the transverse direction (along T-tubules). RyR indicates ryanodine receptors.

(consistent with major:minor axis slopes of 1.6 for clusters and 1.2 for Ca^{2+} sparks; Figure 2C versus Figure S6D).

Peak amplitude and mean spark intensity were also used to reduce false-positive events (Figure S6A through S6C). The spatial profiles of peaks for raw fluorescence signals $\Delta F/F_0$ (gray) or after applying a Gaussian fit on the raw profile (red) or after applying a 2D Gaussian filter (blue) showed that this method provides accurate localization of Ca^{2+} spark peaks.

Colocalization of Ca^{2+} Sparks and RyR Cluster Sites

To determine the RyR cluster size (Figure 1E) for each site of Ca^{2+} spark initiation, we detected the Ca^{2+} spark peak locations (Figure 4A) and correlated these locations to the nearest RyR cluster center in the same Z-plane near the middle of the cell (described in more detail in Figure 5). Each white dot in Figure 4B indicates the peak location of every Ca^{2+} spark measured in the whole time series (600 frames), with an enlarged region in Figure 4Bb. The peaks of sparks are mainly located along Z-lines (arrow 1), but "hot" regions for spontaneous sparks are seen (arrow 2), and some sparks appear between Z-lines in the longitudinal direction (arrow 3). In Figure 4C through 4E, we reported quantitative results for (N=10) cells of the fraction of Ca^{2+} sparks as a function of the distance to the nearest RyR cluster (Figure 4C) and, when normalized, by the area of the disk where the spark is detected (Figure 3D) because for radii >0, the area for apparent spark sites increases as r^2. We also plotted probability of spark occurrence versus distance to the nearest Z-line (Figure 4E) and found that 90% of sparks are within 0.5 μm of the Z-line (cumulative probability). We expected tighter proximity, based on prior line-scan Ca^{2+} spark measurements with F-FKBP[9] or GFP-tagged RyR2,[31] but the 12.5-millisecond 2D imaging frequency required here may add uncertainty with respect to precise location of the initiation site.

Figure 5A shows a representative confocal FKBP12.6 fluorescence image (top) where we derived "Z-lines" by skeletonizing the binary mask after thresholding (middle). The Fluo-4 image was obtained by averaging all the time series frames (bottom). The superimposition of the Z-lines and average Fluo-4 image (Figure 5Bb), where each green dot represents a Ca^{2+} spark peak location, shows the location of both apparent spark origination site and Z-lines. Figure 5C shows that the majority of Ca^{2+} spark occurrence follows the cluster distribution, peaking between $\Delta F/F_0$ of 0.5 to 2.5 (see

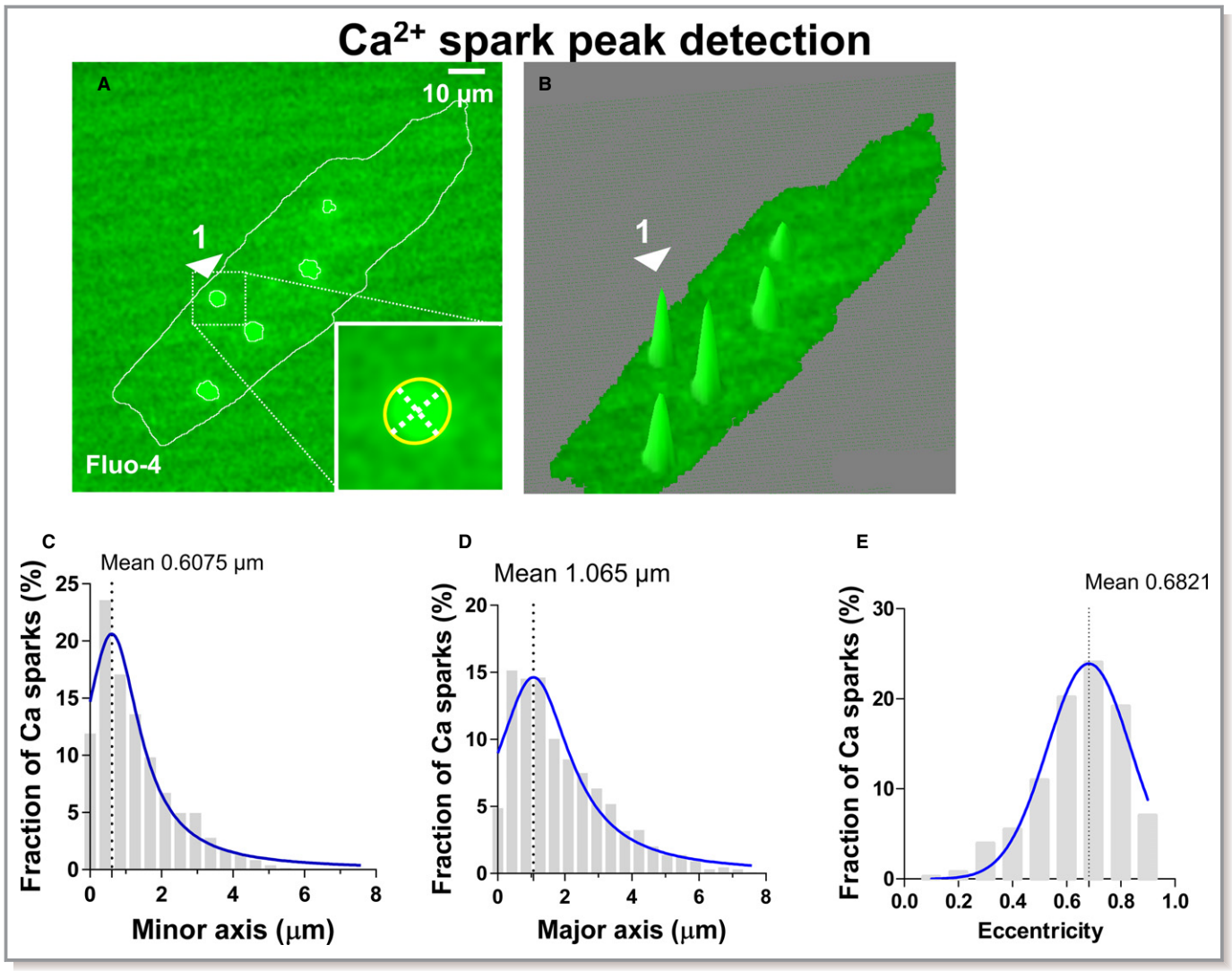

Figure 3. Ca^{2+} spark peak detection. A, Representative confocal Fluo-4 fluorescence frame extracted from 600 sequential frames. White outline indicates cell border, and yellow outlines indicate sparks detected for this frame (inset shows enlargement of region 1) with major and minor axes depicted. B, 3-Dimensional surface plot of the same frame as in A with the signal over the spark threshold detection shown. The threshold is set at 1 standard deviation above the local mean intensity. C and D, Distribution of Ca^{2+} spark major axis and minor axis lengths (N=8 cells, n=1 rat, Lorentzian fit). E, Distribution of spark shape eccentricity (see also RyR cluster eccentricity in Figure S5, Gaussian fit). RyR indicates ryanodine receptors.

Figure 1D), with similar FKBP dependence (for clusters within 0.5-1 μm of Z-line; n=10 myocytes). For clusters right at the Z-line, this is shifted to larger RyR numbers (blue).

The true impact of RyR cluster size on individual clusters is masked in Figure 5C because there are so few large clusters ($\Delta F/F_0$ >3; Figure 1D), so their contribution to overall Ca^{2+} spark frequency is small. We correct for this in Figure 5D by normalizing for fraction of RyRs at each cluster-size bin. For the optimally assigned Z-line sparks, there is a clear dependence of Ca^{2+} spark frequency on the number of RyRs per cluster (Figure 5D). The curves for relaxed Z-line stringency (within 0.5 μm) were similar in shape. So, although there are fewer sites with clusters >3 $\Delta F/F_0$, larger clusters are more likely to fire Ca^{2+} sparks.

Figure 6A combines the Z-line data from Figure 5D with RyR calibrations from Figure 1D and 1E. What is striking here is that sites with ≤60 RyRs have very low propensity for Ca^{2+} sparks but that this probability rises monotonically, and nearly linearly, between 90 and 200 RyRs per cluster. The apparent threshold for Ca^{2+} spark occurrence near 70 RyRs per cluster could mean that the Ca^{2+} sparks from smaller clusters are smaller in amplitude and are thus poorly detected. However, Ca^{2+} spark amplitude was already large at quite small RyR clusters (≈20) and did not change significantly over the full range of cluster sizes (Figure 6B). This has 2 major implications. First, it suggests that a normal Ca^{2+} spark amplitude can be supported by a relatively small number of local RyRs (as few as 8-10), and this makes it functionally adequate to

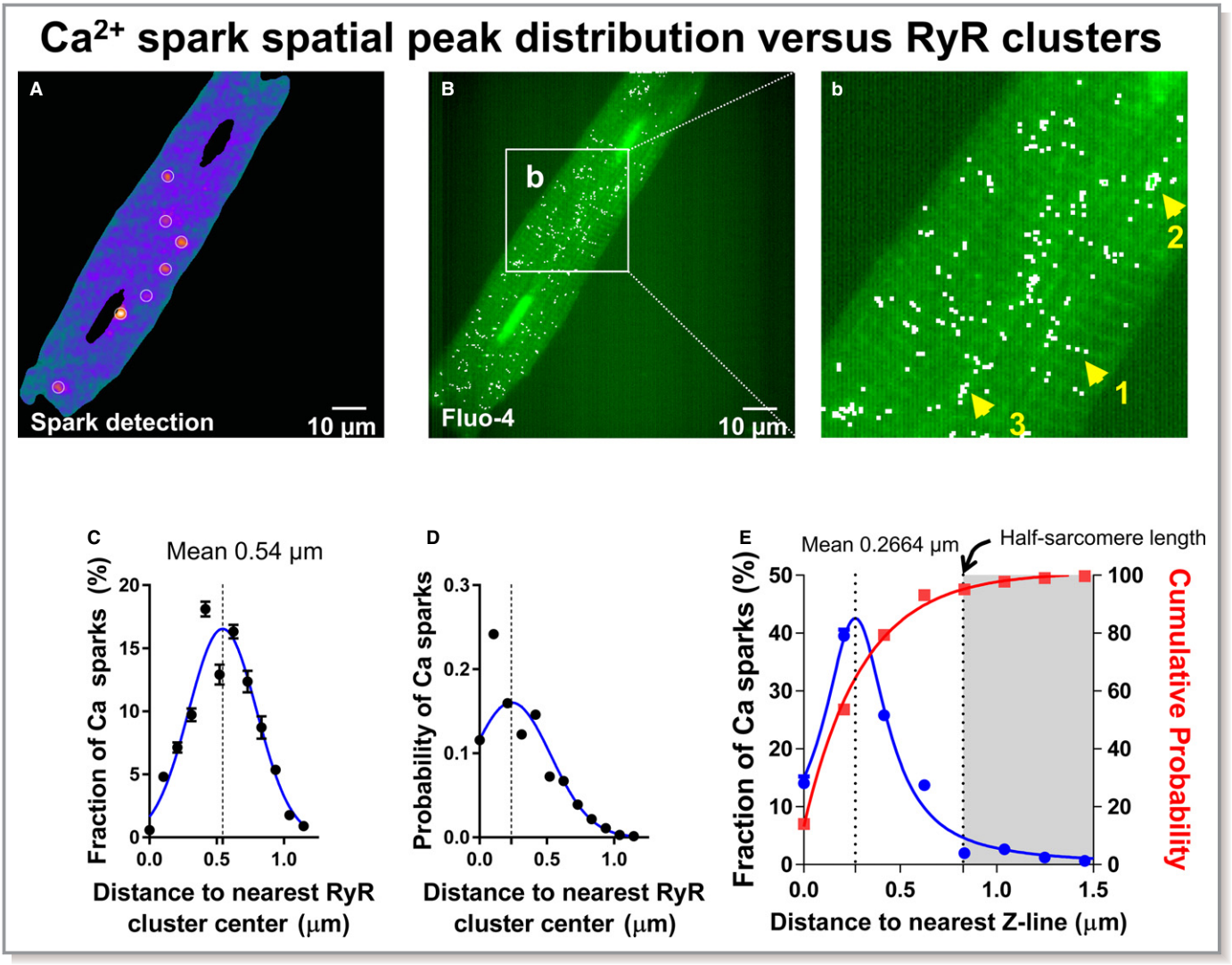

Figure 4. Ca^{2+} sparks spatial distribution vs RyR clusters. A, Representative Ca^{2+} spark frame with detected peak locations circled in white. B, Each white dot indicates the peak location of each Ca^{2+} spark in the whole series of 600 frames. Bb, Enlargement showing sparks typically located along Z-lines (arrow 1), but also at hot spots (arrow 2) and some between Z-lines (arrow 3). C through E, Quantitative results obtained for n=10 cells, N=2 rats showing the fraction of Ca^{2+} sparks vs distance to nearest RyR cluster (C) when corrected for larger area at larger distances (blue line: Gaussian fit) (D), and vs distance to Z-line with cumulative Ca^{2+} spark probability superimposed (blue line, Lorentzian fit; red line, 1 phase association fit) (E). D, This panel shows the fraction of Ca^{2+} spark normalized by the area of the disk where the spark is detected. RyR indicates ryanodine receptors.

have modest-sized clusters at certain sites, with a severalfold safety margin at most junctions during excitation-contraction (E-C) coupling. Second, the amount of SR Ca^{2+} released during a Ca^{2+} spark (or at a given junction during normal E-C coupling) is relatively independent of the number of RyRs per junction over a very broad range.

Does This Match Expectations From Mathematical Models?

We then tested whether our experimental results are consistent with our prior mathematical descriptions of Ca^{2+}-spark genesis via local CICR within a cluster and with termination regulated by both cleft $[Ca^{2+}]_i$ and $[Ca^{2+}]_{SR}$.[18] Figure 6C shows single-junction simulations for a physiologically relevant $[Ca^{2+}]_{SR}$ (650-700 μmol/L) as a function of RyR cluster size (smooth curves). These simulations (without tuning of our prior model) match reasonably well with key results of our experiments, including the very low Ca^{2+}-spark frequency for small clusters, a steep increase at larger cluster size, and also the relatively modest dependence of Ca^{2+}-spark amplitude on RyR number in the cluster (Figure 5D). This also constitutes a level of validation for our junctional cleft model. Note that altering RyR Ca^{2+} sensitivity (eg, by increasing $[Ca^{2+}]_{SR}$ or RyR phosphorylation or oxidation) shifts these curves left, reducing the apparent threshold that is near 70 RyRs per cluster in

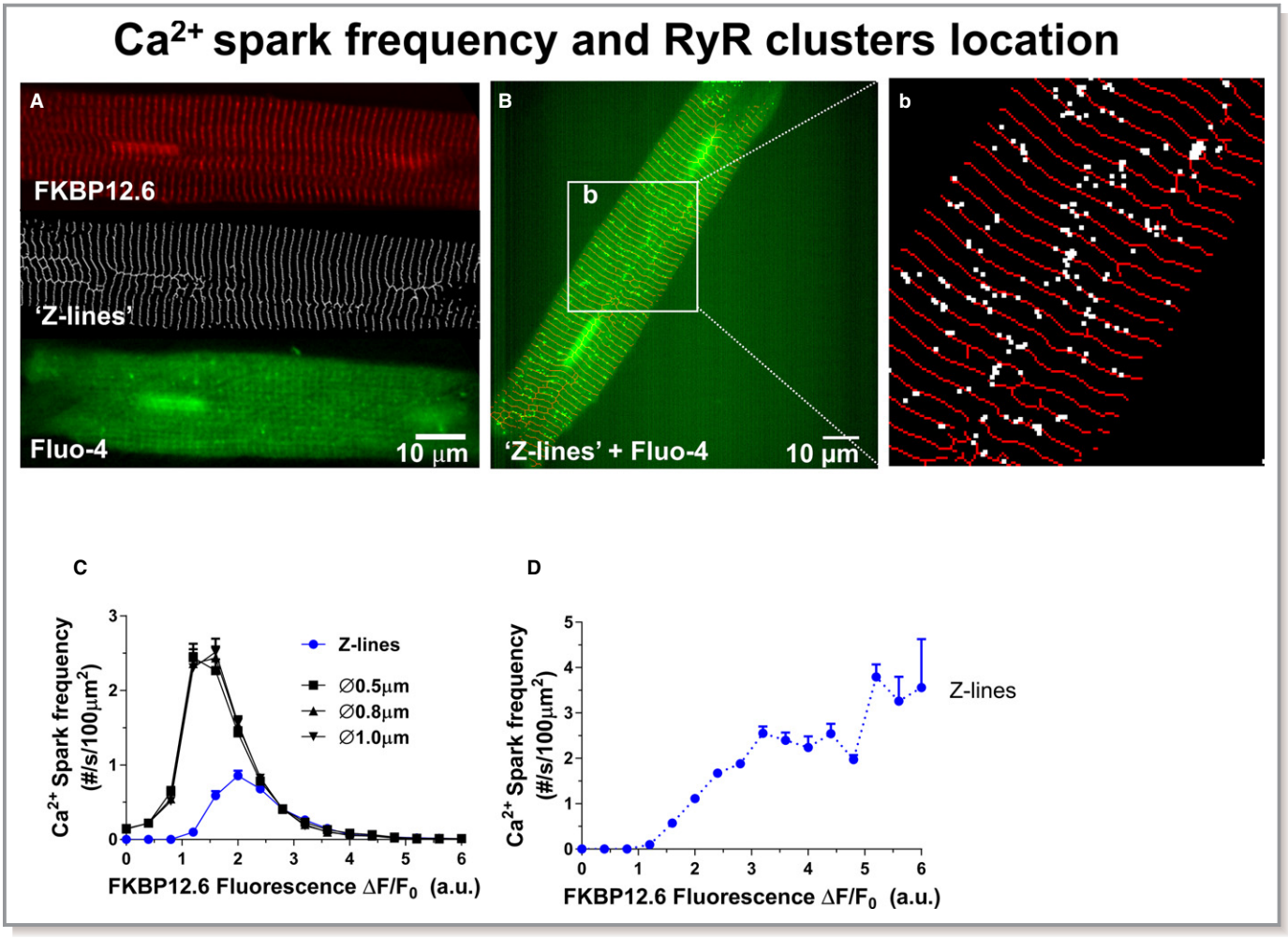

Figure 5. Ca^{2+} Spark frequency and RyR cluster locations. A, Representative confocal FKBP12.6 fluorescence image (top). Z-lines are obtained by skeletonizing binary mask after thresholding (middle). Fluo-4 image is average of all frames from time series (bottom). B, Superimposition of Z-lines and average Fluo-4 image with green dots representing a Ca^{2+} spark peaks. Bb, enlargement (white box) showing only Z-lines and spark peak sites. C, Quantitative results (for n=10 cells, N=2 rats) of overall Ca^{2+} spark frequency as a function of FKBP12.6 fluorescence ($\Delta F/F_0$). D, Same data as in C, but normalized by fraction of RyR clusters (from Figure 1D). RyR indicates ryanodine receptors.

our experiments. Missed events (subthreshold nonspark Ca^{2+} leak) would be expected to have similar dependence on the number of RyRs in Figure 6A and 6C but would make the curves in Figure 6B and 6D more continuous at low amplitude and RyR number. That does not alter our conclusions.

Discussion

This is the first study to simultaneously measure cardiac myocyte Ca^{2+} sparks and the RyR cluster size that underlies those fluxes. This combination allowed direct identification of the number of RyRs per cluster at specific Ca^{2+}-spark sites within the myocyte. This provides explicit information about how the number of RyRs per cluster or junction influences local SR Ca^{2+} release during both Ca^{2+} sparks and normal E-C coupling.

Major Findings and Implications

Our key findings include that Ca^{2+}-spark frequency depends directly on RyR cluster size but that Ca^{2+}-spark amplitude does not (at least above a threshold cluster size). Moreover, modest-sized RyR clusters (<70 RyRs per cluster) dramatically limit the propensity for diastolic Ca^{2+} sparks and leak, and therefore arrhythmogenic Ca^{2+} waves. However, even a small RyR cluster (8-10 RyRs per cluster) is capable of producing a normal-sized SR Ca^{2+}-release event. During normal E-C coupling, the L-type Ca^{2+} channel (I_{Ca}) can synchronously and reliably activate nearly all junctions in a normal myocyte.[32] This is because normally the local I_{Ca} provides a strong enough local CICR signal at the junction to ensure multiple RyR openings to ignite the full-blown Ca^{2+}-release event.[18] So there is probably an ideal range of RyRs per junction that creates a safety margin to assure effectiveness of E-C coupling, perhaps several times the

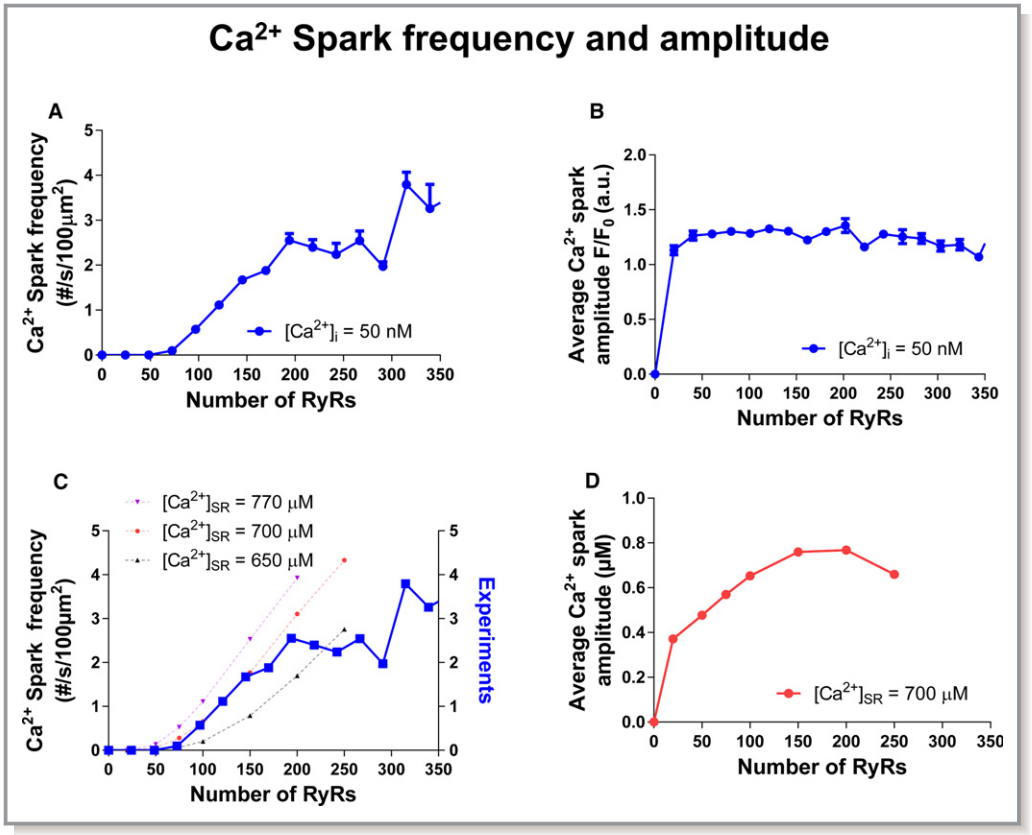

Figure 6. Ca^{2+} Spark frequency and amplitude as function of RyR cluster size. A and B, Ca^{2+} spark frequency (A) and amplitude (B) from experimental data with abscissa transformed to RyR numbers (based on Figure 1E). C and D, Simulations of RyR cluster size effect on Ca^{2+} spark frequency and amplitude at steady state with $[Ca]_{SR}$=700, 770, and 650 μmol/L (with experimental data from (A) (blue). RyR indicates ryanodine receptors; SR, sarcoplasmic reticulum.

minimal number of 6 to 10 RyRs (eg, ≈50 RyRs). This coincides with the most common junction sizes (60-120; Figure 1D). It would also make for reliable E-C coupling and at the same time limit diastolic SR Ca^{2+} leak. However, $[Ca^{2+}]_{SR}$ is a critical regulator of SR Ca^{2+}-release fidelity; so to have a safety margin over a range of physiological conditions, this ideal range might be closer to 100 RyRs per cluster. The flip side of this E-C coupling safety margin is that when SR Ca^{2+} content, cleft $[Ca^{2+}]_I$, or RyR sensitivity is elevated, the curves in Figure 6C would be shifted to the left and upward, which could strongly promote arrhythmogenic Ca^{2+} leak and waves.[16,18] But as we have seen, under normal conditions there are few clusters large enough to be effective in recruiting Ca^{2+} waves.

Ca^{2+}-spark amplitude was surprisingly independent of the number of RyRs per cluster between 20 and 300 RyRs per cluster (Figure 5B). A larger number of RyRs at 1 junction could certainly increase the rate of SR Ca^{2+} release because flux rate should be proportional to the number of open channels (N_o) times the driving $[Ca^{2+}]$ gradient ($[Ca^{2+}]_{SR}-[Ca^{2+}]_{Cleft}$). However, that expected larger release flux is tempered by the decrease of both driving force (reduced $[Ca^{2+}]_{SR}$ and elevated $[Ca^{2+}]_{cleft}$) and the closure of RyR channels that is caused by low local regulatory $[Ca^{2+}]_{SR}$ and progressively weaker activation by $[Ca^{2+}]_{cleft}$ (that is caused by lower driving force and the aforementioned lower N_o).[14,17,18,33,34] Regardless of the detailed molecular mechanism, this relative uniformity of SR Ca^{2+} release is beneficial for E-C coupling. That is, similar SR Ca^{2+} release for junctions of different sizes and locations will tend to produce spatially uniform Ca^{2+} transients across the myocyte (and heart), and that will promote more uniform activation of contraction and cardiac pumping efficiency. Regional differences would result in less-well-activated regions being stretched by well-activated regions, thereby limiting cardiac pressure development and ejection.

Overall, the intrinsic effects of RyR cluster size variation on Ca^{2+}-spark frequency and amplitude as measured here seem largely beneficial under physiological conditions. However, pathological conditions such as heart failure with altered RyR sensitization[1] and structure cluster and T-tubule–SR organization[35-40] could undermine these intrinsically beneficial effects and contribute to cardiac dysfunction and arrhythmogenesis.

Technical Aspects

To obtain simultaneous F-FKBP/RyR and $[Ca^{2+}]_i$ data, we used live-cell confocal imaging for both. This created trade-offs in spatial resolution of RyR cluster size versus that attainable via superresolution or electron microscopy, and also for Ca^{2+} sparks versus line scanning. Optimization of these measurements allowed adequate direct identification of RyR clusters that underlie individual Ca^{2+} sparks, making our specific aim achievable.

Higher RyR spatial resolution can be reached in fixed cells (eg, via dSTORM), but that precludes simultaneous Ca^{2+}-spark imaging. Line-scan confocal imaging could enhance temporal details of Ca^{2+} sparks (≈2 ms/line), but the 1-dimensional nature limits the spatial information obtained (and would not help for RyR localization). We improved our confocal RyR cluster resolution in the Ca^{2+}-spark plane by adding longer scan times (to improve signal-to-noise ratio) and deconvolution of Z-stack images. We also used F-FKBP, which contains a single fluorophore per molecule that binds stoichiometrically (1:1 per RyR monomer) with subnanomolar affinity and that approach enhances quantitative inferences.[9]

We optimized Ca^{2+}-spark detection by a new 2D automated spark analysis method. Even so, Ca^{2+}-spark initiation sites might occur out of the plane of focus, and with 12.5 ms/image, the geometrical peak of the Ca^{2+}-spark signal might be slightly missed. We did find that the apparent Z-lines were remarkably well aligned vertically in Z-stack images, so that cannot explain off–Z-line spark sites. We also corrected for drift in the x-y plane (Figure S7D). Overall, our approach provides good estimates of both Ca^{2+}-spark peak locations and local RyR cluster sizes. However, we cannot rule out that some Ca^{2+} sparks initiate slightly out of the focal plane and that smaller RyR clusters may exist within the domains that we identify as a single RyR cluster.

RyR Clusters Versus Superclusters and Ca^{2+} Release Units

High-resolution imaging has shown that RyR clusters can range from 1 to 400 per cluster,[2-6] but terminology merits further discussion. Seminal quantitative electron microscopy by Franzini-Armstrong et al[4] inferred a typical RyR cluster in rat ventricular myocyte junctions to be 267 in circular arrays, requiring a fully packed checkerboard array of 553 nm diameter (for 30-nm center-center RyR distance).[41,42] The value of 267 RyRs per cluster may be at the high end of normal for 3 reasons. First, in heart there are often drop-outs from these arrays, to the point where there are often multiple smaller RyR clusters that are within 100 nm of each other.[3,5] These groups of clusters (or superclusters) are often at the same junctional cleft but lie transversely along Z-lines and could also span adjacent junctions. Second, many junctions are smaller than 560 nm in diameter and so cannot physically hold that many RyRs. Third, if the overall number of RyRs per 30-pL rat myocyte (≈2.5 million) were distributed to 20 000 junctions,[30] each would have 126 RyRs (requiring 380-nm diameter junctions).

These overall constraints are consistent with our calibration (Figure 1E) where mean cluster size is 84 RyRs, and most clusters are between 15 and 212 RyRs ($\Delta F/F_0$ between 0.25 and 3.5 and diameter 0.25–0.76 μm). What we are calling clusters in our study are probably similar to the superclusters of Hou et al,[5] which averaged 103 RyRs and included on average 3.4 clusters. We think that our clusters likely constitute the functional SR Ca^{2+}-release units that underlie the observed Ca^{2+} sparks, and that the true number of RyRs is within ≈25% of our inferred number. We might miss a small number of tiny clusters that are distant from identified clusters, but ≈90% of all Z-line clusters are within 200 nm of other clusters.[5] Although the vast majority of interior RyRs and Ca^{2+}-spark initiation sites are near Z-lines, some RyR clusters and sparks are observed at other cellular loci (eg, sarcomeric, near mitochondria, and perinuclear).[31,43,44]

Dependence of Ca^{2+} Sparks on RyR Cluster Size

Our experiments and model here showed that Ca^{2+}-spark frequency increases with RyR cluster size, but not appreciably until >70 RyRs per cluster (Figure 6). This differs from some prior modeling predictions.[35,45] Walker et al[45] predicted that Ca^{2+}-spark frequency should rise steeply at very few RyRs per cluster starting at 1 RyR per cluster and then flatten off for clusters >50. Macquaide et al[35] predicted that Ca^{2+}-spark frequency would decrease with increasing RyR cluster size. These discrepancies are likely because of fundamental model assumptions (eg, simple 2-state RyR model with allosteric RyR-RyR coupling in clusters).[35,45] We use a 4-state Markov RyR model in which RyRs function independently, with activation and inactivation governed by local cleft and intra-SR $[Ca^{2+}]$.[18,46] Our model seems to better replicate the measured RyR per cluster dependence of Ca^{2+}-spark frequency and amplitude (Figure 6).

Conclusion

In this study, we developed a new method to simultaneously detect Ca^{2+} sparks and RyR cluster size in ventricular myocytes. This allowed us to measure the influence of a broad range of RyRs per cluster on Ca^{2+}-spark frequency and amplitude. Modest-sized clusters (10-50 RyRs) are able to produce full-sized SR Ca^{2+}-release events when triggered during E-C coupling but have a very low probability of producing arrhythmogenic diastolic Ca^{2+} sparks and waves. Larger RyR clusters (>75) progressively increase the

probability of diastolic Ca^{2+} sparks and have an increased likelihood of being local initiators of pathological SR Ca^{2+} leaks. This would synergize with analogous effects of increased SR Ca^{2+} and diastolic $[Ca^{2+}]_i$ loading and post-translational RyR sensitization (eg, via phosphorylation or redox modulation).

Acknowledgments

We thank Dr Razvan Cornea (University of Minnesota, Minneapolis, MN) for providing the fluorescent FKBP12.6 for our studies.

Author Contributions

All authors contributed to the conception and design of the study, interpretation of the data, and writing of the manuscript. Yang and Galice performed the experimental work. Galice analyzed the results. Xie performed the simulations. All authors have approved the version to be published. Dr Yang's current institution is Lingnan Medical Research Center, Guangzhou University of Chinese Medicine.

Sources of Funding

This work was supported by National Institutes of Health grants R01-HL30077, R01-HL092097, and R01-HL105242 (Bers), R00-HL111334 (Sato), American Heart Association grant 16GRNT31300018 (Sato), and Amazon AWS Cloud Credits for Research (Sato).

Disclosures

None.

References

1. Bers DM. Cardiac sarcoplasmic reticulum calcium leak: basis and roles in cardiac dysfunction. *Annu Rev Physiol*. 2014;76:107–127.
2. Asghari P, Scriven DR, Sanatani S, Gandhi SK, Campbell AI, Moore ED. Nonuniform and variable arrangements of ryanodine receptors within mammalian ventricular couplons. *Circ Res*. 2014;115:252–262.
3. Baddeley D, Jayasinghe ID, Lam L, Rossberger S, Cannell MB, Soeller C. Optical single-channel resolution imaging of the ryanodine receptor distribution in rat cardiac myocytes. *Proc Natl Acad Sci USA*. 2009;106:22275–22280.
4. Franzini-Armstrong C, Protasi F, Ramesh V. Shape, size, and distribution of Ca^{2+} release units and couplons in skeletal and cardiac muscles. *Biophys J*. 1999;77:1528–1539.
5. Hou Y, Jayasinghe I, Crossman DJ, Baddeley D, Soeller C. Nanoscale analysis of ryanodine receptor clusters in dyadic couplings of rat cardiac myocytes. *J Mol Cell Cardiol*. 2015;80:45–55.
6. Hayashi T, Martone ME, Yu Z, Thor A, Doi M, Holst MJ, Ellisman MH, Hoshijima M. Three-dimensional electron microscopy reveals new details of membrane systems for Ca^{2+} signaling in the heart. *J Cell Sci*. 2009;122:1005–1013.
7. Bers DM. Cardiac excitation-contraction coupling. *Nature*. 2002;415:198–205.
8. Cordeiro JM, Spitzer KW, Giles WR, Ershler PE, Cannell MB, Bridge JH. Location of the initiation site of calcium transients and sparks in rabbit heart Purkinje cells. *J Physiol*. 2001;531:301–314.
9. Guo T, Cornea RL, Huke S, Camors E, Yang Y, Picht E, Fruen BR, Bers DM. Kinetics of FKBP12.6 binding to ryanodine receptors in permeabilized cardiac myocytes and effects on Ca sparks. *Circ Res*. 2010;106:1743–1752.
10. Parker I, Zang WJ, Wier WG. Ca^{2+} sparks involving multiple Ca^{2+} release sites along Z-lines in rat heart cells. *J Physiol*. 1996;497(Pt 1):31–38.
11. Mackenzie L, Bootman MD, Berridge MJ, Lipp P. Predetermined recruitment of calcium release sites underlies excitation-contraction coupling in rat atrial myocytes. *J Physiol*. 2001;530:417–429.
12. Chen-Izu Y, McCulle SL, Ward CW, Soeller C, Allen BM, Rabang C, Cannell MB, Balke CW, Izu LT. Three-dimensional distribution of ryanodine receptor clusters in cardiac myocytes. *Biophys J*. 2006;91:1–13.
13. Dries E, Bito V, Lenaerts I, Antoons G, Sipido KR, Macquaide N. Selective modulation of coupled ryanodine receptors during microdomain activation of calcium/calmodulin-dependent kinase II in the dyadic cleft. *Circ Res*. 2013;113:1242–1252.
14. Picht E, Zima AV, Shannon TR, Duncan AM, Blatter LA, Bers DM. Dynamic calcium movement inside cardiac sarcoplasmic reticulum during release. *Circ Res*. 2011;108:847–856.
15. Wu X, Bers DM. Sarcoplasmic reticulum and nuclear envelope are one highly interconnected Ca^{2+} store throughout cardiac myocyte. *Circ Res*. 2006;99:283–291.
16. Zima AV, Bovo E, Bers DM, Blatter LA. Ca^{2+} spark-dependent and -independent sarcoplasmic reticulum Ca^{2+} leak in normal and failing rabbit ventricular myocytes. *J Physiol*. 2010;588:4743–4757.
17. Zima AV, Picht E, Bers DM, Blatter LA. Termination of cardiac Ca^{2+} sparks: role of intra-SR $[Ca^{2+}]$, release flux, and intra-SR Ca^{2+} diffusion. *Circ Res*. 2008;103:e105–e115.
18. Sato D, Bers DM. How does stochastic ryanodine receptor-mediated Ca leak fail to initiate a Ca spark? *Biophys J*. 2011;101:2370–2379.
19. Yang Y, Guo T, Oda T, Chakraborty A, Chen L, Uchinoumi H, Knowlton AA, Fruen BR, Cornea RL, Meissner G, Bers DM. Cardiac myocyte Z-line calmodulin is mainly RyR2-bound, and reduction is arrhythmogenic and occurs in heart failure. *Circ Res*. 2014;114:295–306.
20. Cornea RL, Nitu F, Gruber S, Kohler K, Satzer M, Thomas DD, Fruen BR. FRET-based mapping of calmodulin bound to the RyR1 Ca^{2+} release channel. *Proc Natl Acad Sci USA*. 2009;106:6128–6133.
21. Guo T, Fruen BR, Nitu FR, Nguyen TD, Yang Y, Cornea RL, Bers DM. FRET detection of calmodulin binding to the cardiac RyR2 calcium release channel. *Biophys J*. 2011;101:2170–2177.
22. Banyasz T, Chen-Izu Y, Balke CW, Izu LT. A new approach to the detection and statistical classification of Ca^{2+} sparks. *Biophys J*. 2007;92:4458–4465.
23. Steele EM, Steele DS. Automated detection and analysis of Ca^{2+} sparks in x-y image stacks using a thresholding algorithm implemented within the open-source image analysis platform ImageJ. *Biophys J*. 2014;106:566–576.
24. Schneider CA, Rasband WS, Eliceiri KW. NIH image to ImageJ: 25 years of image analysis. *Nat Methods*. 2012;9:671–675.
25. Vonesch C, Terrés Cristofani R, Schmitt G. 3D deconvolution package for microscopic images. http://bigwww.epfl.ch/deconvolution/. Lausanne, Switzerland: 2008.
26. Kirshner H, Sage D. A Java software package to generate realistic 3D microscope point-spread function (PSF). http://bigwww.epfl.ch/algorithms/psfgenerator/. Lausanne, Switzerland: 2014.
27. Soeller C, Crossman D, Gilbert R, Cannell MB. Analysis of ryanodine receptor clusters in rat and human cardiac myocytes. *Proc Natl Acad Sci USA*. 2007;104:14958–14963.
28. Jayasinghe ID, Crossman DJ, Soeller C, Cannell MB. A new twist in cardiac muscle: dislocated and helicoid arrangements of myofibrillar z-disks in mammalian ventricular myocytes. *J Mol Cell Cardiol*. 2010;48:964–971.
29. Bers DM, Stiffel VM. Ratio of ryanodine to dihydropyridine receptors in cardiac and skeletal muscle and implications for E-C coupling. *Am J Physiol*. 1993;264:C1587–C1593.
30. Bers DM. *Excitation-Contraction Coupling and Cardiac Contractile Force*. Dordrecht, the Netherlands: Kluwer Academic Publishers; 2001.
31. Hiess F, Vallmitjana A, Wang R, Cheng H, ter Keurs HE, Chen J, Hove-Madsen L, Benitez R, Chen SR. Distribution and function of cardiac ryanodine receptor clusters in live ventricular myocytes. *J Biol Chem*. 2015;290:20477–20487.
32. Inoue M, Bridge JH. Ca^{2+} sparks in rabbit ventricular myocytes evoked by action potentials: involvement of clusters of L-type Ca^{2+} channels. *Circ Res*. 2003;92:532–538.
33. Gillespie D, Fill M. Pernicious attrition and inter-RyR2 CICR current control in cardiac muscle. *J Mol Cell Cardiol*. 2013;58:53–58.
34. Cannell MB, Kong CH, Imtiaz MS, Laver DR. Control of sarcoplasmic reticulum Ca^{2+} release by stochastic RyR gating within a 3D model of the cardiac dyad

and importance of induction decay for CICR termination. *Biophys J*. 2013;104:2149–2159.

35. Macquaide N, Tuan HT, Hotta J, Sempels W, Lenaerts I, Holemans P, Hofkens J, Jafri MS, Willems R, Sipido KR. Ryanodine receptor cluster fragmentation and redistribution in persistent atrial fibrillation enhance calcium release. *Cardiovasc Res*. 2015;108:387–398.
36. Wu HD, Xu M, Li RC, Guo L, Lai YS, Xu SM, Li SF, Lu QL, Li LL, Zhang HB, Zhang YY, Zhang CM, Wang SQ. Ultrastructural remodelling of Ca^{2+} signalling apparatus in failing heart cells. *Cardiovasc Res*. 2012;95:430–438.
37. Chen-Izu Y, Ward CW, Stark W Jr, Banyasz T, Sumandea MP, Balke CW, Izu LT, Wehrens XH. Phosphorylation of RyR2 and shortening of RyR2 cluster spacing in spontaneously hypertensive rat with heart failure. *Am J Physiol Heart Circ Physiol*. 2007;293:H2409–H2417.
38. Heinzel FR, Bito V, Biesmans L, Wu M, Detre E, von Wegner F, Claus P, Dymarkowski S, Maes F, Bogaert J, Rademakers F, D'Hooge J, Sipido K. Remodeling of T-tubules and reduced synchrony of Ca^{2+} release in myocytes from chronically ischemic myocardium. *Circ Res*. 2008;102:338–346.
39. Louch WE, Mork HK, Sexton J, Stromme TA, Laake P, Sjaastad I, Sejersted OM. T-tubule disorganization and reduced synchrony of Ca^{2+} release in murine cardiomyocytes following myocardial infarction. *J Physiol*. 2006; 574:519–533.
40. Song LS, Sobie EA, McCulle S, Lederer WJ, Balke CW, Cheng H. Orphaned ryanodine receptors in the failing heart. *Proc Natl Acad Sci USA*. 2006;103:4305–4310.
41. Franzini-Armstrong C. Can the arrangement of RyR2 in cardiac muscle be predicted? *Biophys J*. 2016;110:2563–2565.
42. Cabra V, Murayama T, Samso M. Ultrastructural analysis of self-associated RyR2s. *Biophys J*. 2016;110:2651–2662.
43. Lukyanenko V, Ziman A, Lukyanenko A, Salnikov V, Lederer WJ. Functional groups of ryanodine receptors in rat ventricular cells. *J Physiol*. 2007;583:251–269.
44. Rajagopal V, Bass G, Walker CG, Crossman DJ, Petzer A, Hickey A, Siekmann I, Hoshijima M, Ellisman MH, Crampin EJ, Soeller C. Examination of the effects of heterogeneous organization of RyR clusters, myofibrils and mitochondria on Ca^{2+} release patterns in cardiomyocytes. *PLoS Comput Biol*. 2015;11:e1004417.
45. Walker MA, Williams GS, Kohl T, Lehnart SE, Jafri MS, Greenstein JL, Lederer WJ, Winslow RL. Superresolution modeling of calcium release in the heart. *Biophys J*. 2014;107:3018–3029.
46. Shannon TR, Wang F, Puglisi J, Weber C, Bers DM. A mathematical treatment of integrated Ca dynamics within the ventricular myocyte. *Biophys J*. 2004;87:3351–3371.

SUPPLEMENTAL MATERIAL

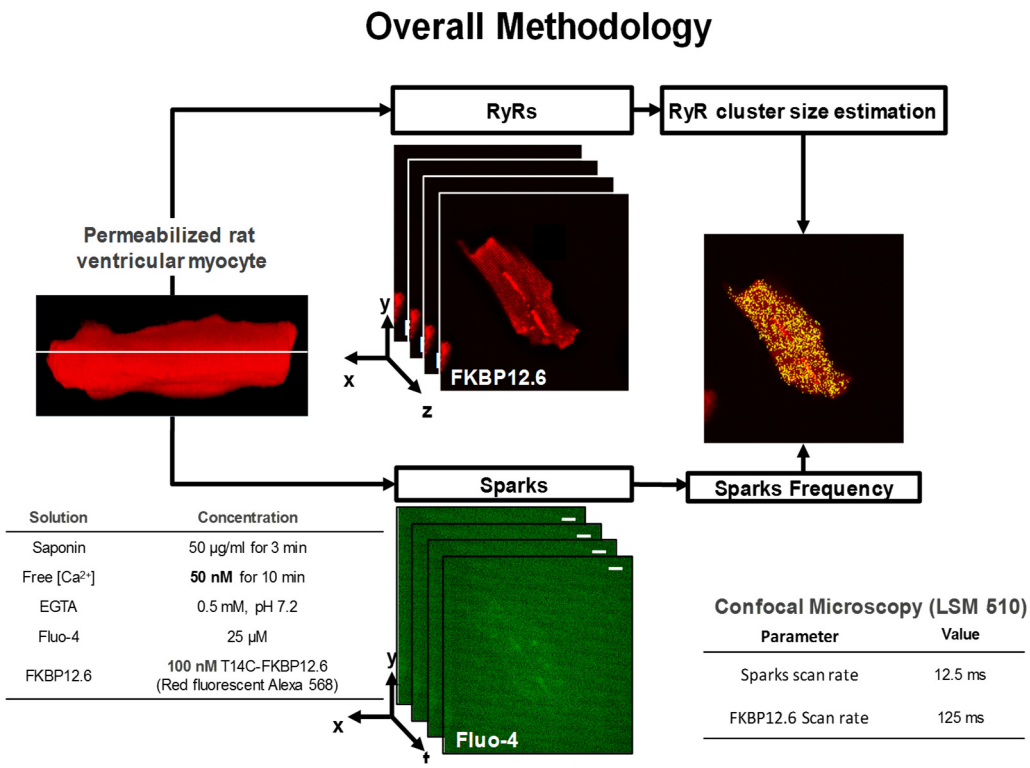

Figure S1. Overall methodology. Permeabilized rat ventricular cardiac myocytes are labeled with two markers. F-FKBP12.6 is used to localize and characterize the RyR clusters. Fluo-4 is used as an indicator of Ca^{2+} spark activity. Image processing is used to analyze the data and determine the relationship between spark frequency and RyR cluster size.

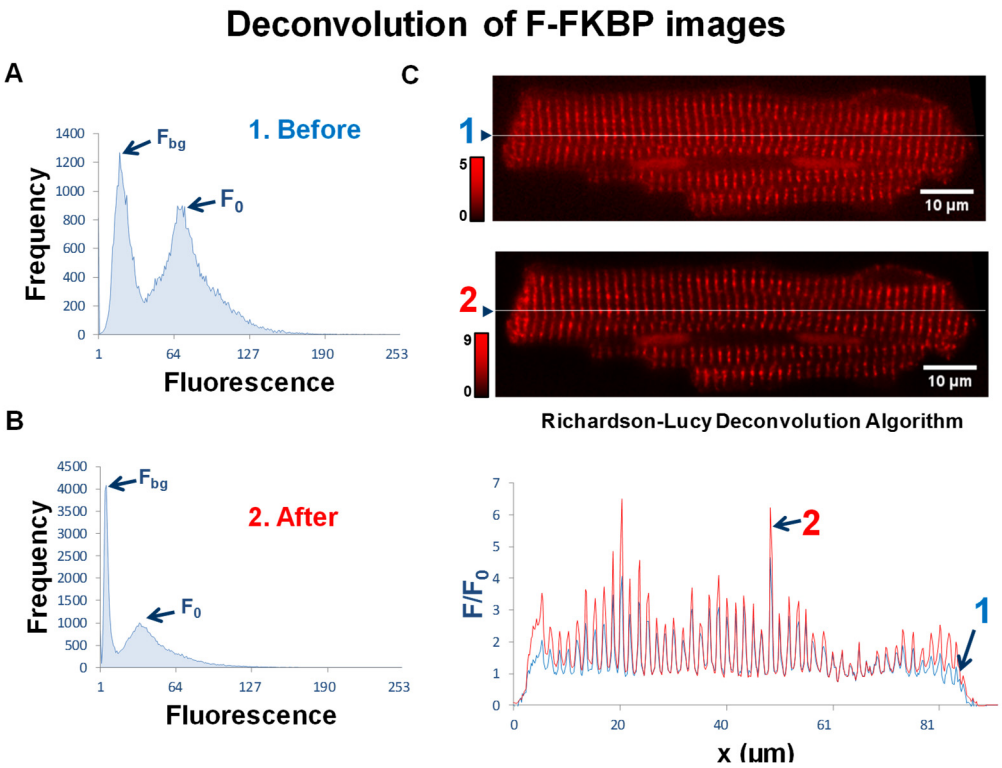

Figure S2. Estimation of the size of RyR cluster from FKBP12.6 confocal z-stack. (A-B) Frequencies of FKBP12.6 total fluorescence before (A) and after (B) applying a Richardson-Lucy deconvolution filter. F_{bg} and F_0 indicate respectively the fluorescence value of the background and the baseline. **(C)** Profiles of FKBP12.6 relative fluorescence F/F_0 before (blue) and after (red) deconvolution which improves the detection of RyR cluster.

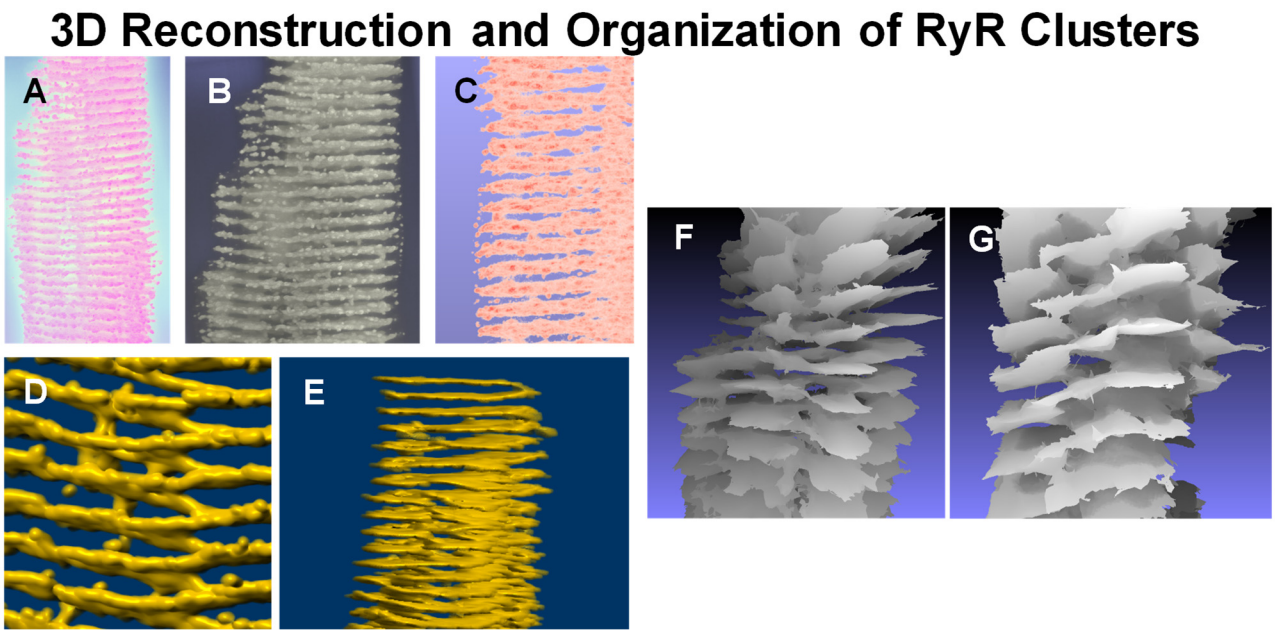

Figure S3. 3D reconstruction and organization of RyR clusters in a rat ventricular cardiac myocyte. (A-C) RyR clusters are in different false color renderings (A-B). Raw z-stack images were deconvolved using a theoretical point spread function based on the optical system. The color or transparency depends on FKBP12.6 fluorescence intensity. RyR clusters at the surface are visible (C) and can be een to intercalate between Z-lines. **(D-G)** Internal structure of the RyR clusters are shown (D-E), using a threshold to segment visible/opaque regions. Helicoid staircases are clearly visible. Using a finite element mesh reconstruction (F-G) shows that RyR clusters form a complex structure.

3D Myocyte Reconstructions and Estimating RyR numbers

A 3D Reconstruction

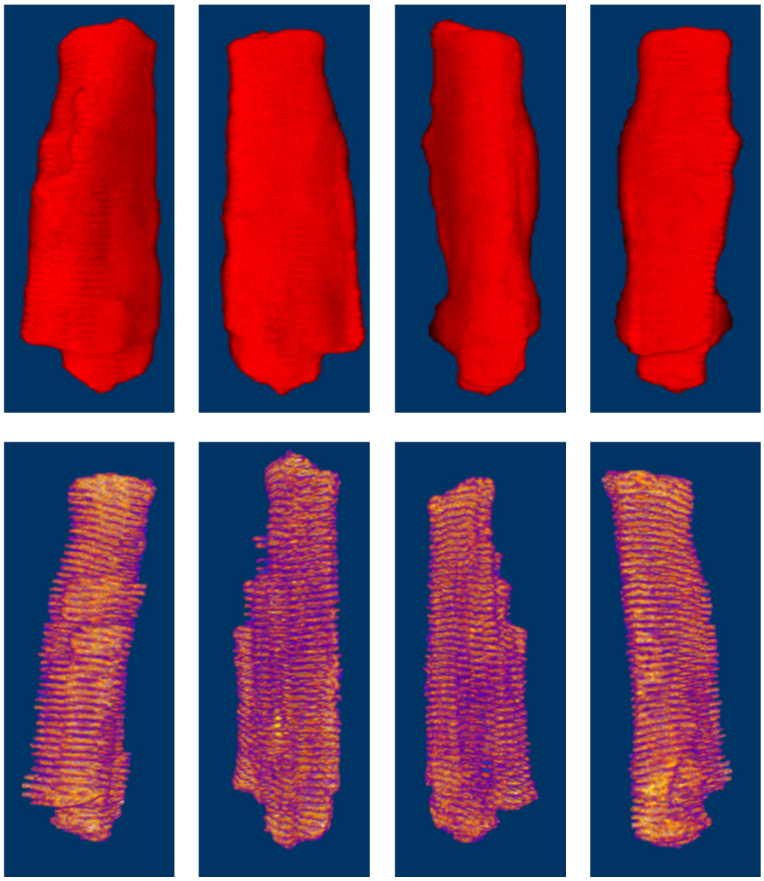

B. Estimating RyR numbers in Myocyte

$$\left(\frac{833\ \text{fmol RyR*}}{\text{mg cell protein}}\right)\left(\frac{168\ \text{mg cell protein**}}{\text{ml cytosol}}\right)\left(\frac{10^3\ \text{ml}}{\text{L}}\right)\left(\frac{\mu\text{mol}}{10^9\ \text{fmol}}\right) = \frac{0.1399\ \mu\text{mol}}{\text{L cytosol}} = \frac{140\ \text{nmol RyR}}{\text{L cytosol}}$$

$$\left(\frac{140\ \text{nmol RyR*}}{\text{L cytosol}}\right)\left(\frac{6.02\times10^{23}}{\text{mole}}\right)\left(\frac{10^{-9}\ \text{mol}}{\text{nmol}}\right)\left(\frac{10^{-12}\ \text{L}}{\text{pL}}\right) = \frac{84{,}300\ \text{RyR}}{\text{pL cytosol}} = \frac{84.3\ \text{RyR}}{\mu\text{m}^3\ \text{cytosol}}$$

*from ^{3}H-ryanodine binding measurement in isolated rat ventricular myocyte homogenates (Bers DM & Stiffel VM. Ratio of ryanodine to dihydropyridine receptors in cardiac and skeletal muscle and implications for E-C coupling. *Am J Physiol*. 264:C1687-C1593, 1993)

**from Table 9 in Bers (Bers, D. M. Excitation-Contraction Coupling and Cardiac Contractile Force. Kluwer Academic Press, Dordrecht, Netherlands, 2001). The basis is the 1.83-fold and 1.66-fold purification of dihydropyridine and ryanodine receptors in isolated myocytes (Bers & Stiffel, 1993) yielding the product [0.574 mg cell pn/mg vent homog pn][120 mg homog pn/g wet wt][2.43 kg wet wt/L cytosol]=168 g cell pn/L cytosol.

Thus, average cytosolic F-FKBP $\Delta F/F_0$ (per μm^3) should equal 84.3 RyRs. These calculations also imply ~2.5 million RyR tetramers in a 30 pL rat ventricular myocyte. This [RyR] is similar to our titration of high affinity (K_d =0.70 nM) F-FKBP12.6 binding sites (B_{max} =0.92 μM for RyR monomers, or 0.23 μM for full RyR tetramers). Another constraint is that for a RyR array of 400 nm diameter the maximum number of RyR tetramers would be ~160 (for tightest possible packing) or 80 (for full checkerboard packing). Thus, while are estimates for the calibration are approximate, they are reasonably constrained by other work.

Figure S4. 3D Myocyte Reconstructions and Estimating RyR numbers (A)
3D reconstruction of a cell based on the FKBP12.6 z-stack series (top). After removing background signal and correcting for baseline signal (F_0), we extract voxels for each cluster (bottom) **(B)** Calculations used to infer appropriate estimated calibration of FKBP12.6 relative fluorescence ($\Delta F/F_0$) to the number of RyR tetramers that it represents.

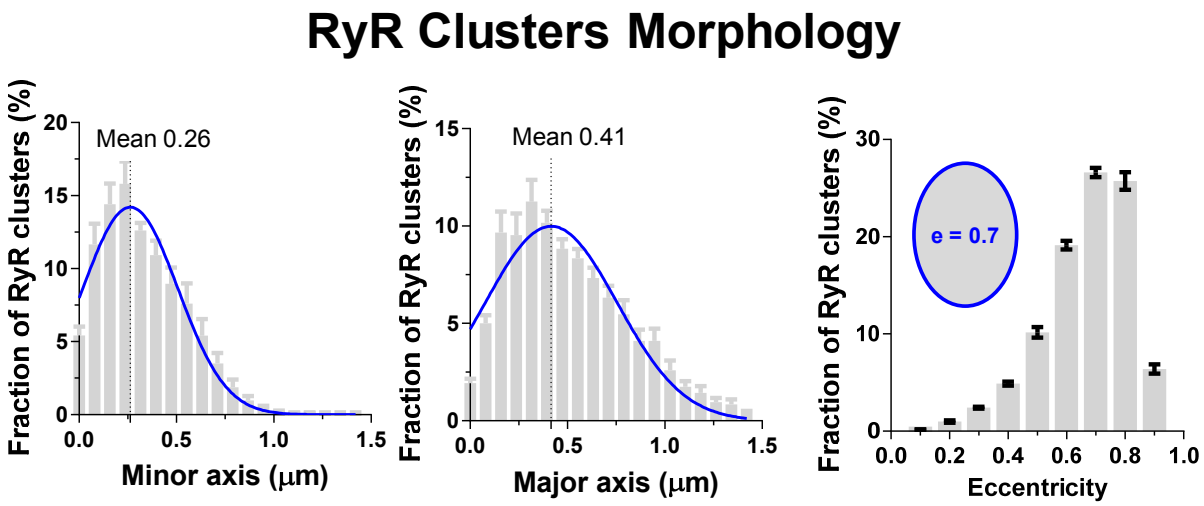

Figure S5. RyR cluster Morphology. Frequency histograms of shapes of FKBP12.6 (or RyR) lusters (as identified in Fig 1B). The shapes are typically not strictly elliptical, but major and minor axes were measured (a and b, respectively; left and middle) and the eccentricity of each cluster was calculated ($e=\sqrt{(1-a^2/b^2)}$) to provide an index of asymmetry (n=8 cells, N=1 rat, Gaussian fit).

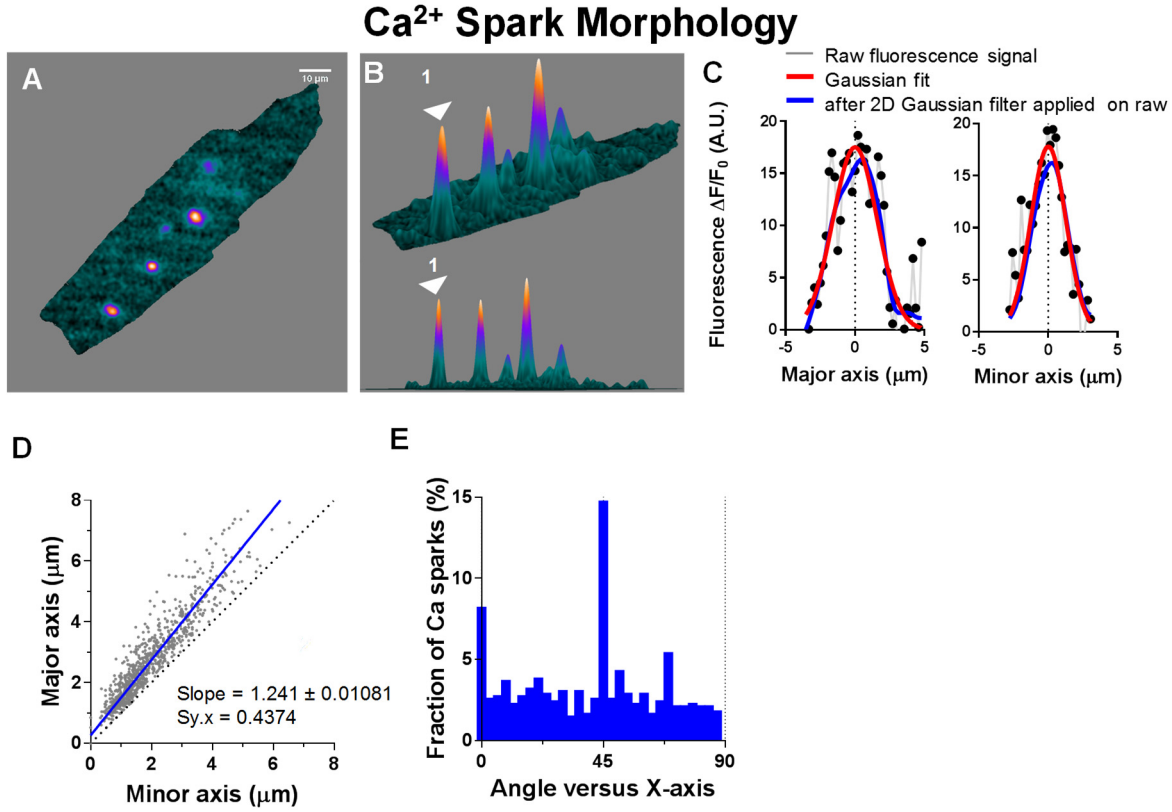

Figure S6. Refinement of Ca^{2+} spark Morphology. (**A-B**) Peak amplitude and mean intensity were used to reduce false-positive events and obtain clear Ca^{2+} spark profiles, viewed in the x-y plane (A) and from an oblique and side angle (showing intensity in both color and height). (**C**) Spatial profiles for raw $\Delta F/F_0$ (gray) and after applying a simple Gaussian fit on the raw profile (red) or after applying a 2D Gaussian filter (blue). This method provides accurate localization of Ca^{2+} spark peaks. (**D**) The shape of Ca^{2+} sparks. Major axis vs Minor axis. The slope was 1.24±0.01, which indicates slightly ellipsoidal (n=4 cells, N=1 rat, Linear regression fit). (**E**) Distribution of Ca^{2+} spark orientation. This graph shows that there is no preferred orientation.

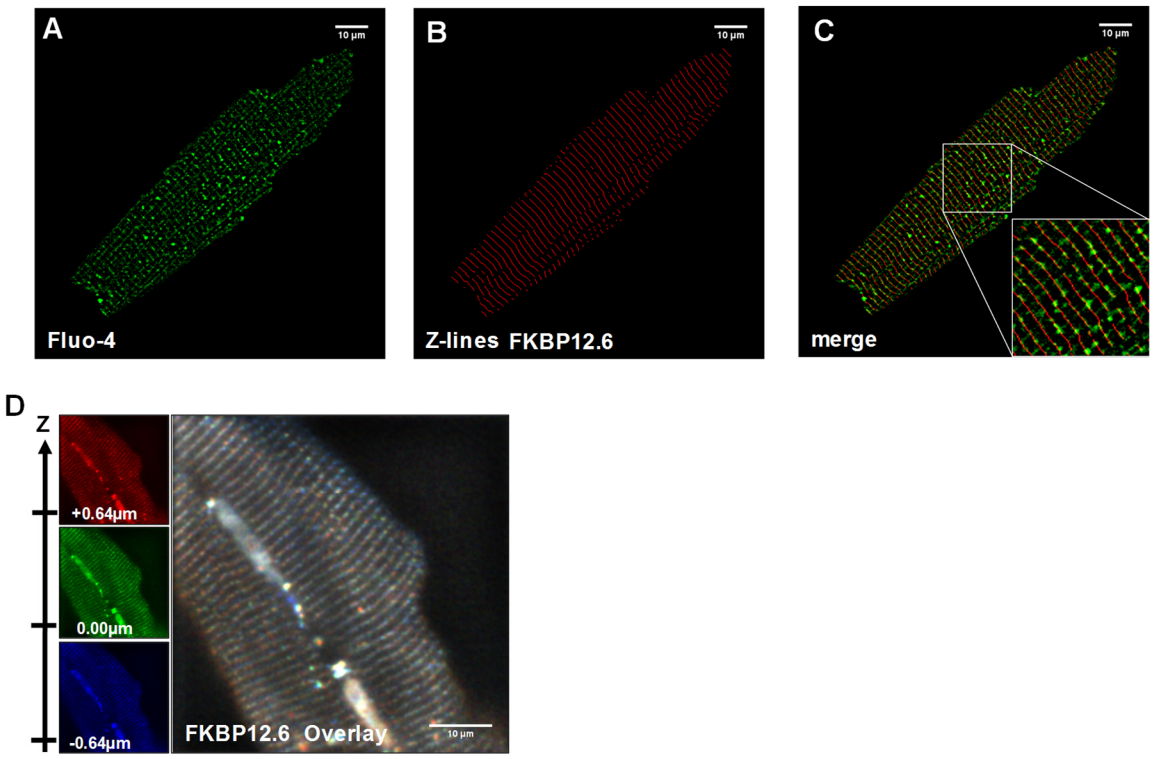

Figure S7. Limited Spatial and Focal Drift. Representative images of the mean intensity of the confocal Fluo-4 time series (**A**) recorded within the same focal plane as the confocal FKBP12.6 (**B**) and merged (**C**) indicate no noticeable difference in the x-y plane. (**D**) **Red**, green and blue images (left) **are at** different z-planes (+0.64, 0, -0.64 µm). The merged image shows little change in the structure for these three planes (white color). This indicates that within this depth (relevant to our analysis here), the Z-lines and RyRs are well aligned. This limits the impact of F-FKBP sites above and below the spark plane from influencing the x-y plane analysis.